ACS Catalysis

Research Article

pubs.acs.org/acscatalysis

Reaction Mechanism of Human Renin Studied by Quantum Mechanics/Molecular Mechanics (QM/MM) Calculations

Ana R. Calixto, Natércia F. Brás, Pedro A. Fernandes, and Maria J. Ramos*

REQUIMTE/Departamento de Química e Bioquímica, Faculdade de Ciências, Universidade do Porto, Rua do Campo Alegre s/n, 4169-007 Porto, Portugal

Supporting Information

ABSTRACT: In this paper, we present the catalytic mechanism of human renin computationally investigated using an ONIOM quantum mechanics/molecular mechanics (QM/MM) methodology (B3LYP/6-31G(d):AMBER), with final energies calculated at the M06/6-311++G-(2d,2p):AMBER level of theory. It was demonstrated that the full mechanism involves three sequential steps: (i) a nucleophilic attack of a water molecule on the carbonyl carbon of the scissile bond, resulting in a very stable tetrahedral gem-diol intermediate; (ii) a protonation of the peptidic bond nitrogen; and (iii) a complete breakage of the scissile bond. The activation energy barrier obtained for the angiotensinogen hydrolysis by renin was calculated as 22.0 kcal mol^{-1}, which is consistent with the experimental value, albeit slightly larger. We have shown also that the cleavage of a mutated substrate (Val10Phe) occurs in a manner similar to that of the wild-type substrate. These results provide an understanding of the reaction catalyzed by human renin with atomistic detail. This is of particular importance because this enzyme plays a special role in the control of the renin−angiotensin system and, consequently, it is at the center of current hypertension therapy.

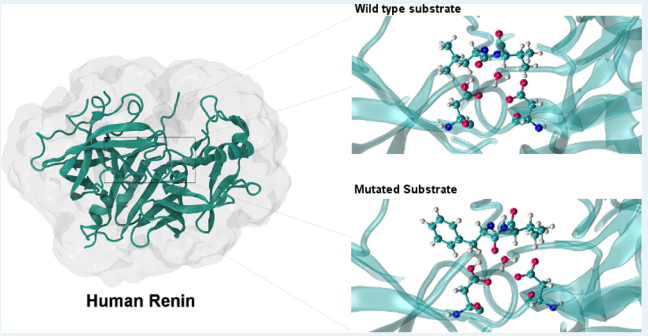

KEYWORDS: *hypertension, renin, QM/MM, ONIOM, catalytic mechanism*

INTRODUCTION

This work explores the catalytic mechanism of human renin with atomic-level detail. Computational methods have been employed for that purpose. Behind the fundamental biochemical knowledge that is gained, the results also facilitate the discovery of new inhibitors with therapeutic potential.

The Renin Angiotensin System (RAS) is the principal regulator of fluid homeostasis and blood pressure. This multienzymatic cascade system begins with a two-step hydrolysis of the angiotensinogen peptide. In the first enzymatic reaction, angiotensinogen is cleaved by renin, resulting in the release of the decapeptide angiotensin I (Ang I). Subsequently, the angiotensin converting enzyme (ACE) hydrolyses Ang I, releasing the two terminal residues and generating the octapeptide angiotensin II (Ang II), which is an agonist of the AT1 receptor that, when activated, induces an increase in blood pressure.

Excessive activation of this system leads to an increase in blood pressure and, consequently, hypertension, which currently is a very important worldwide public health challenge.[1−6]

The hydrolysis of angiotensinogen carried out by renin constitutes the rate-limiting step of the RAS cascade.[7−10] The cleavage takes place between two residues, leucine and valine, and releases the 10 N-terminal residues generating Ang I, which is the only substrate for renin[2,3,11,12] that is known to man. As such, renin is a very attractive target to control the blood pressure. Intervention at this level of the RAS cascade is more specific than intervention more downstream, such as at the ACE enzyme or AT_1 receptor, as no other metabolic pathway is affected. The first inhibition of renin available over the counter (Aliskiren) reached the market only in 2007, even though the research of bioavailable inhibitors of renin has begun many decades ago.[13] Unfortunately, Aliskiren is associated with significant side effects. Therefore, studies on renin are very important to promote future studies on its inhibition.[14−16]

Renin: The Relationship between Structure and Function. The monomeric protease renin (EC 3.4.23.15), a member of the aspartic protease superfamily,[17] has 340 residues (molecular weight of 40 kDa). This enzyme consists of two similar β-sheets lobes with dissimilar sequences. As in many other aspartic proteases, between these lobes, there is a deep cleft where the active site is located, burying seven substrate residues.

This active site has two essential, coplanar, aspartic acid residues (Asp38 and Asp236), emanating from different lobes, whose conformation is stabilized by a network of hydrogen bonds. The carboxyl groups are hydrogen-bonded to a water

Received: April 15, 2014
Revised: September 2, 2014
Published: September 3, 2014

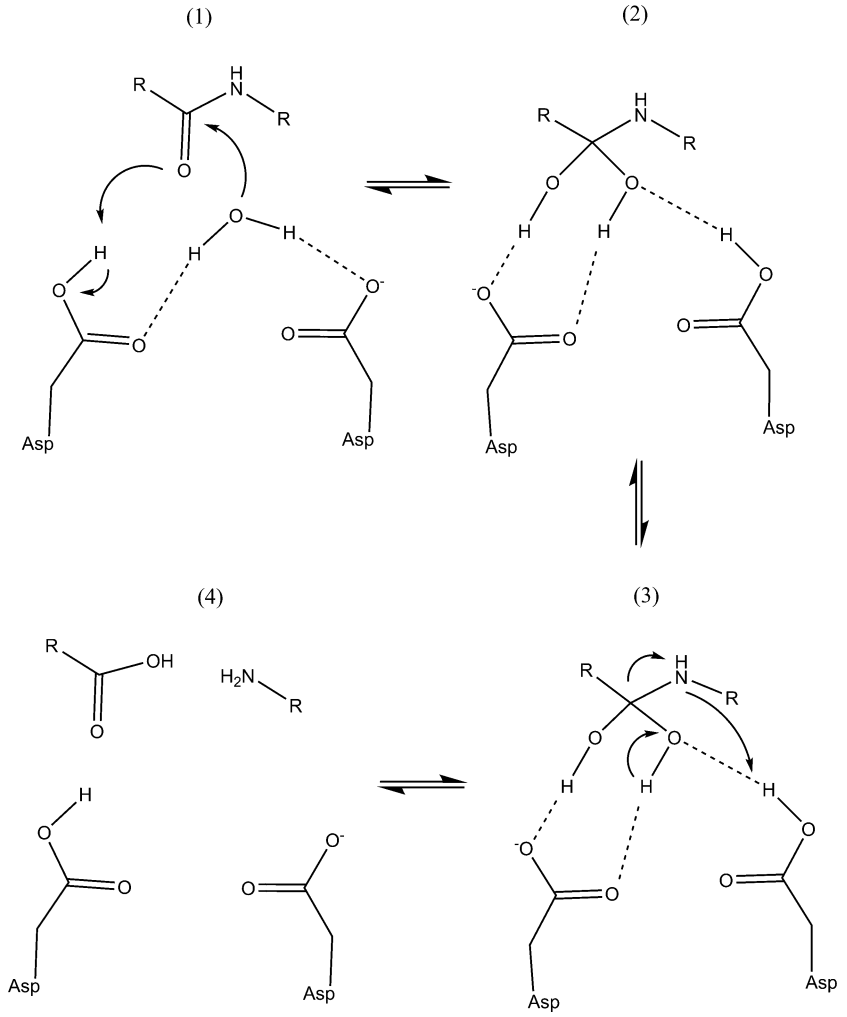

Figure 1. General representation of the catalytic mechanism proposed for aspartic proteases. The catalytic water molecule is tightly bound to the catalytic aspartates (**1**). In the first step, a gem-diol tetrahedral intermediate is formed (**2**). The breaking of the C−N bond is accompanied by the transfer of a proton to the nitrogen of the leaving amino group (**3** and **4**).

molecule that is essential for renin catalytic activity. Its position close to the substrate, polarized by one aspartate residue, is fundamental for the catalytic mechanism of renin.[3,16,18−20] Renin has a flexible flap close to the active site. An identical structure is also common in other aspartic proteases, and it allows covering the active site upon substrate binding. Recent molecular dynamics (MD) studies on this enzyme showed that this flap oscillates between an open, semiopen, and close conformation. This behavior is important to allow the binding of the substrate and an extensive range of different inhibitors.[5,21−23]

Mechanism Proposed for Aspartic Proteases. *β*-secretase, HIV-1 protease, presenilin, and other aspartic proteases have had the details of their catalytic mechanisms described by previous quantum mechanics/molecular mechanics (QM/MM) and MD simulations.[24,25] The catalytic mechanism of renin was also previously proposed as a case of acid−base catalysis, similar to what has been published for other proteases of this family. However, support for the proposal is based just on the similarities between enzyme family members, and the atomistic details of this reaction have not been described until now.

One of the consequences of the close position of the two aspartates is that the pK_a of one of them is increased and the other one is decreased, originating different protonation states for each of them (one protonated and other deprotonated).[25] The postulated mechanism assumes that the catalytic water molecule, which is tightly bound in the active site, is activated by the negatively charged aspartic residue that acts as a general base. Consequently, a nucleophilic attack to the scissile peptidic bond is carried out by the pseudo-hydroxide ion generated *in situ*, giving rise to a gem-diol intermediate. Subsequently, the peptidic nitrogen of the scissile bond is protonated by the second catalytic aspartate and simultaneously a gem-diol hydroxyl is deprotonated by the first, resulting in the cleavage of the peptidic bond (see Figure 1).[25−28]

Consequences of a Leu10Phe Mutation at the Substrate, During the Catalytic Mechanism of Human Renin. The replacement of a leucine by a phenylalanine at the 10th position of the angiotensinogen, which corresponds to the site of the renin cleavage, is related to the emergence of a hypertensive disorder that is common in pregnancy (pre-eclampsia).[29] Because of the importance of this link, we chose to study also the details of the corresponding catalytic mechanism of human renin in the presence of the Leu10Phe-mutated substrate.

dx.doi.org/10.1021/cs500497f | *ACS Catal.* 2014, 4, 3869−3876

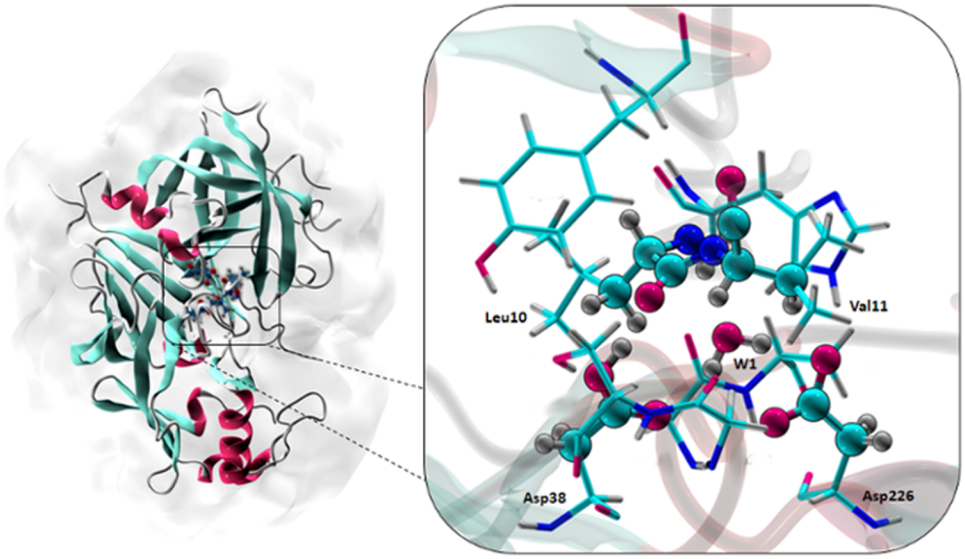

Figure 2. QM/MM model used in the calculations. The optimization of the geometries along the reaction coordinate was performed with 33 atoms in the high layer at the B3LYP 6-31G(d) level (represented by balls and sticks). Single-point energy calculations were done with a larger high level layer (138 atoms), which was treated with different density functionals (B3LYP, M06, B1B95, and mPWB1K) at the 6-311++G(2d,2p) level of theory (licorice representation).

METHODOLOGY

The X-ray structure of unbound human renin (PDB ID: 2REN, 2.5 Å resolution), was used as starting structure for the present study.[17] The substrate was modeled from a lower resolution structure of renin bound to angiotensinogen (PDB ID: 2X0B, 4.4 Å resolution)[30] and corresponded to the Val3-Asp14 residues. We aligned and superimposed both structures from the PDB 2X0B file and transferred the modeled substrate. In the active site, between the catalytic aspartates (Asp38 and Asp226), a water molecule was added. The software X-leap[31] was used to protonate the complex, assuming physiological protonation states for all residues. According to the proposed mechanism for aspartic proteases,[25] one of two catalytic aspartates (Asp38) is protonated at the beginning of the reaction; therefore, we protonated this residue. Eight sodium counterions were added with X-leap to compensate for the negative charge of the system. The system was surrounded by a cubic box of TIP3P water molecules having a minimum distance of 12 Å between the protein atoms and the end of the box.

A two-stage minimization of the geometry using MM (parm99 force field) was performed in order to eliminate clashes and bad contacts. The first stage involved only water molecules and counterions, keeping fixed the position for the protein atoms. In the second stage all atoms were geometry-optimized. The potential energy surface (PES) for the postulated reaction mechanism was explored at the QM/MM level with the Gaussian 09 software.[32] The reactant state was taken from the previously minimized structure, upon deletion of all water molecules beyond a shell of 5 Å around the enzyme−substrate complex. All counterions were far to distant from the active site and, therefore, were removed.

We have employed the ONIOM[33] method as implemented in Gaussian 09. The system was partitioned into two layers: a "high layer", treated at the DFT level, and a "low layer", treated at the classical MM level. Different layer divisions and theoretical levels were considered during geometry optimizations and single-point energy calculations. The first were performed with a small high layer (33 atoms) at the B3LYP 6-31G(d) level of theory (Figure 2), and the low layer with the AMBER parm99 force field. The B3LYP functional was employed as it has been shown to provide accurate results for organic molecules.[34−36] We used hydrogen as link atoms whenever covalent bonding spanned the QM/MM boundaries, in order to saturate the dangling bonds. The system was further divided into a frozen region and a free region. The free region included all the residues that have at least one atom within a 20 Å radius around any atom of the high layer. The remaining atoms, which were located at the periphery, were kept frozen. The interaction between layers was treated with a mechanical embedding scheme.

Linear scans along the reaction coordinates for each mechanistic step were carried out, starting with 0.10 Å increments to locate the relevant transition states, and subsequently finer 0.05 Å increments were made to refine the transition-state geometry. Finally, a full optimization of the transition states was performed, starting from the higher points of the preliminary scans. Atomic point charges for the high layer atoms were determined with the RESP (Restrained Electrostatic Potential) charge fitting program,[37,38] using the Merz−Singh−Kollman scheme[39] at each scan step. These PES scans started from a fully optimized structure of the reactants. The intermediates and products were located also through unconstrained geometry optimizations.

Therefore, all stationary points were geometry optimized and the transition state and minima structures were verified by vibrational frequency calculations having exactly one and none imaginary frequencies, respectively. We have calculated also the zero-point energy, the entropy and the thermal corrections for the change from 0 to 298.15 K, which allowed us to obtain the Gibbs energies at physiological temperature. All these calculations were carried out at the B3LYP/6-31G(d):AMBER level of theory. However, to compare the barriers between the wild-type and the Leu10Phe mutant, we used the PES profiles as approximations, which is accurate enough for comparison purposes. A larger high layer was then selected (a set of

dx.doi.org/10.1021/cs500497f | ACS Catal. 2014, 4, 3869−3876

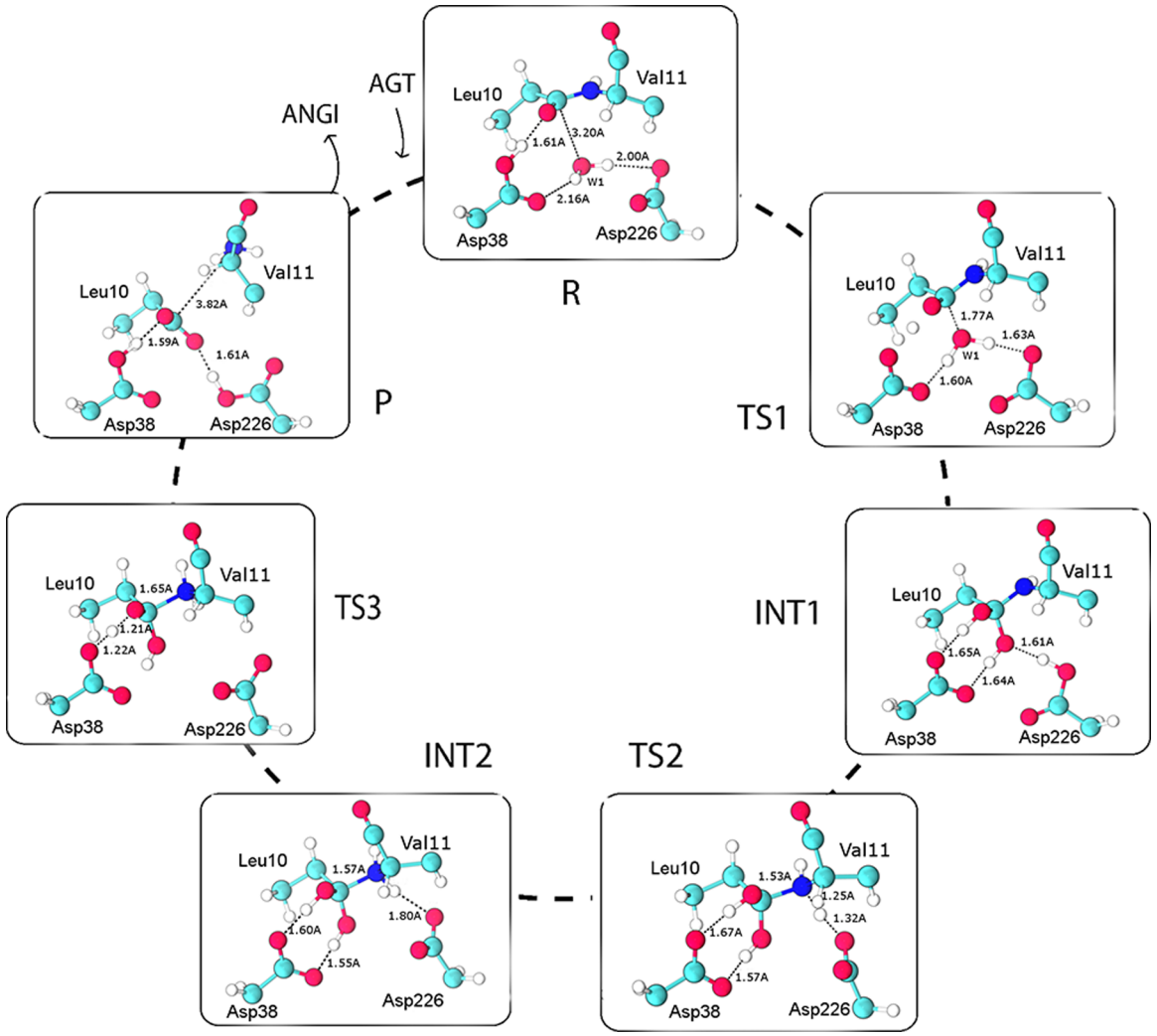

Figure 3. Structures of the reactants, intermediates, transition states and products for the cleavage of the Leu10−Val11 peptide bond of angiotensinogen by human renin. Only the QM-treated atoms are represented in the figure, for the sake of clarity.

residues that participate in the reaction or have important interactions with the active site and the substrate), including 138 atoms (Figure 2). Single-point energy calculations were made subsequently, resorting to the electronic embedding scheme and different density functionals (M06, B1B95, and mPWB1W), whose performance for thermodynamics and kinetics is known to be excellent, together with the larger 6-311++G(2d,2p) basis set.

The energies presented in these work are affected by the used methods and the errors associated with them. From experience with other studies conducted in our group, the errors associated with these methods can influence results in ∼2−4 kcal mol^{-1}.[40−42] These errors may be grounded on several causes, such as the functional chosen, a finite basis set, a high layer with a finite number of atoms, errors associated with MM, the use of a single X-ray structure (that corresponds to an average of all molecules in the crystal), and also a truncated substrate instead of the natural substrate.

RESULTS AND DISCUSSION

As all aspartic proteases, renin hydrolyses peptide bonds by an acid/base mechanism that is supposed to start with the formation of a gem-diol intermediate and to end with the cleavage of the peptide bond. In order to understand the cleavage of the bond between positions 10 and 11 of the dodecapeptide that mimics angiotensinogen, we followed this mechanism with QM/MM calculations.

Hydrolysis of the Wild-Type Substrate. *Structure of the Reactants.* In the structure of the reactants, the active center water molecule was hydrogen-bonded to both catalytic aspartate carboxylates, a conformation adequate for catalysis. Another active site conformation had the two aspartates hydrogen-bonded to each other, but one of the two was protonated. The latter was more stable, but it was not catalytically productive. The difference between the two conformations was small, and the transition between both could be seen easily in MD simulations.[25] Therefore, in the present work, we started from the first productive conformation, and we used the 12 terminal residues that bind the enzyme cleft as a model of the angiotensinogen substrate. At the beginning of the reaction, the carbonyl oxygen of Leu10 (which belonged to the peptide that was to be cleaved), was hydrogen-bonded (1.61 Å) to the carboxylic proton of Asp38 (Figure 3). A hydrogen bond was also formed between the hydroxyl group of Ser41 and the carboxyl group of Asp38, enhancing the acidity of the aspartate. This serine residue was part of a network of hydrogen bonds, involving Tyr83 and Trp45, which stabilizes the active center conformation. The

dx.doi.org/10.1021/cs500497f | ACS Catal. 2014, 4, 3869−3876

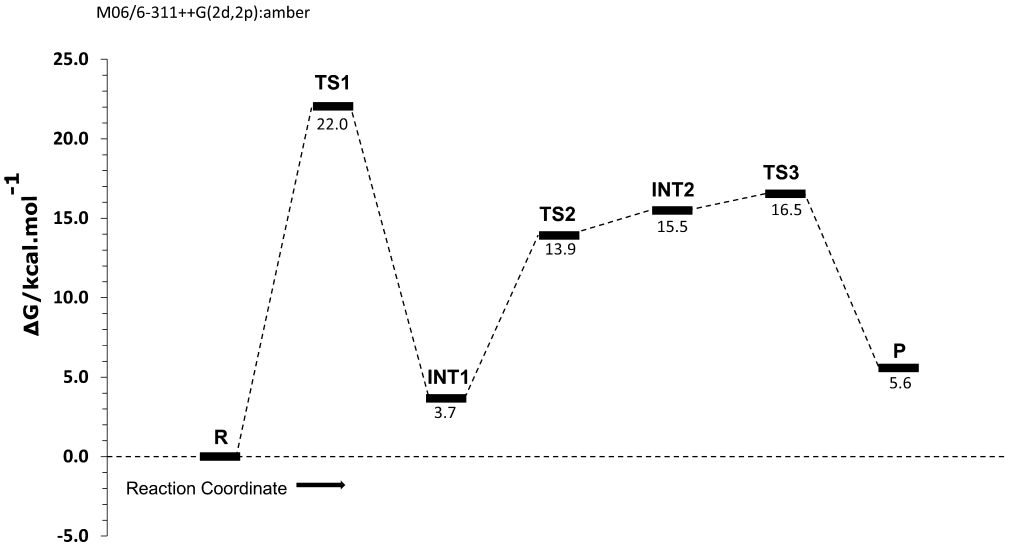

Figure 4. Energetic pathway for the hydrolysis reaction of angiotensinogen catalyzed by human renin at the M06/6-311++G(2d,2p):AMBER level with 138 atoms in the high layer.

initial conformation of the reactive aspartates was also stabilized by hydrogen bonding to two glycine residues (Gly39 and Gly220).

The First Reaction Step: The Nucleophilic Attack of the Catalytic Water Molecule. The catalytic cycle was supposed to begin with the formation of a gem-diol intermediate. As such, the distance between the water oxygen and the carbonyl carbon of the scissile bond was adopted as the reaction coordinate. In the optimized reactants, the catalytic water molecule was trapped between Asp38 and Asp226, establishing hydrogen bonds with bond residues with lengths of 2.00 Å (H_{W1}−O_{Asp226}) and 2.16 Å (H_{W1}−O_{Asp38}). Such interactions, and the protonation states of the catalytic aspartates, provided the correct position of the water molecule to promote the nucleophilic attack to the carbonyl carbon.

After partial deprotonation by Asp226, the resulting hydroxyl anion carried out a nucleophilic attack on the carbonyl carbon of Leu10. Concertedly, Asp38 protonated the Leu10 carbonyl and the Asp226 was protonated by one of the water molecule protons. Full optimization of the transition-state structure and vibrational frequencies analysis revealed just one imaginary frequency (172*i* cm^{-1}) that coincided with the adopted reaction coordinate (O_{W1}−$C_{carbonyl}$ stretching). The distance between O_{W1} and $C_{carbonyl}$ decreased from 3.20 Å to 1.77 Å, when moving from the reactants (R) to TS1, both illustrated in Figure 3. The proton of Asp38 was not fully transferred to the carbonyl oxygen at this stage. In the products of this step, the carboxylate group got protonated and a new covalent bond between the water oxygen and the carbonyl carbon of Leu10 was established. The carbonyl carbon changed from sp_2 to sp_3, and the peptide bond became tetrahedral. As can be seen in Figure 3, this intermediate (INT1) had two hydroxyl groups covalently bonded to the carbon of the scissile bond (gem-diol intermediate). Asp38 and Asp226 both changed their protonation states, and the two hydroxyl groups from the substrate established hydrogen bonds with Asp38 (1.65 and 1.64 Å).

Previous studies have provided indications that the aspartic proteases reactions start by a nucleophilic attack of a water molecule on the scissile bond of the substrate, as we tested in this work. However, the nature of the first intermediate is still a matter of controversy. Some studies indicate that the reaction intermediate resulting from the first step is a neutral gem-diol; other studies suggest that a charged hydroxyl anion is stable in the active site of the proteases. In the present study, we performed a scan in which the water oxygen was pushed against the carbonyl carbon, and the forming oxyanion was spontaneously protonated by Asp38. We did not find a stationary point with the gem-diol ionized and the Asp38 protonated. This result is in agreement with previous studies, which suggest that the neutral gem-diol intermediate is more stable than a charged oxyanion.[43]

The structure of the first intermediate was similar to that described for other members of the aspartic protease family. However, with regard to the TS1 geometry, it was different from that described for other family members, such as BACE-1 or HIV-1 proteases, which involve the formation of a hydroxyl anion at the TS.[24] The other residues around the active center preserved their overall structure along this reaction step. For example, the hydrogen bond network established between Asp38−Ser41−Tyr83−Trp45 was kept intact. However, because of the ionization of Asp38, the hydrogen bond between Ser41 and Asp38 got shortened and the first stabilized the carboxylate group of the latter.

The activation free energy for this step was calculated to be 22.0 kcal mol^{-1} with a large high layer (138 atoms) at the M06/6-311++G(2d,2p):AMBER level of theory (see Figure 4). This value is comparable, albeit higher, to the experimental one obtained for the angiotensinogen hydrolysis by renin (16.5 kcal mol^{-1}).[44]

The Second Reaction Step. The mechanism of reaction for aspartic proteases (HIV-1, β-secretase, and presenilin) was proposed to occur in two steps: first, the formation of a gem-diol intermediate, and second, the breakage of the peptide bond of the substrate.[24,25] These studies showed that the hybridization of the scissile bond carbon (sp_3) placed the amine nitrogen in an orientation that facilitated the attack of the Asp226 carboxyl hydrogen and, consequently, the breakage of the peptide bond and the return of a proton from the gem-diol intermediate to Asp226. In order to describe the second step of renin's catalytic mechanism and taking into account previous studies on aspartic proteases (particularly in mouse renin) we

dx.doi.org/10.1021/cs500497f | *ACS Catal.* 2014, 4, 3869−3876

started the second step using the geometry of the INT1. At this stage the residues, such as Asp226, were preorganized to facilitate the protonation of the nitrogen of the scissile bond. The Asp226 carboxyl proton−peptidic nitrogen distance was taken as reaction coordinate. During this scan, we obtained the geometry of the second transition state and intermediate (TS2 and INT2), which are represented in Figure 3. We optimized the structure of the TS2 and the nature of the transition state was verified by analyzing the vibrational frequencies. We found an imaginary frequency (911*i* cm^{-1}) that corresponded to the stretching of the atoms involved in the adopted reaction coordinate. The transfer of the proton was associated with a free energy barrier of 13.9 kcal mol^{-1} (Figure 4) and took place concomitantly with an increase in the length of the scissile bond.

Some relevant differences between the INT1 and TS2 structures could be seen easily. When the Asp226 acidic proton came closer to the Val11 nitrogen, it broke its hydrogen bond with the gem-diol hydroxyl and changed its rotamer. The Asp226 proton was shared between donor and acceptor at TS2 (distance of 1.25 Å to Leu10 nitrogen and 1.32 Å to the oxygen). The complete transfer of this proton took place only at INT2.

During this second step, the peptidic bond stretched to 1.53 Å at TS2, and to 1.57 Å at INT2 (Figure 3), meaning that the bond did not completely break during this step. In previous studies of other aspartic proteases at the end of the second reaction step, the scissile bond of the substrate had got broken already. Consistently, the deprotonation of one of the gem-diol hydroxyl groups, back to Asp38, was not observed either. Both catalytic aspartates became negatively charged, while the nitrogen of Leu10 became positive. Previous studies on other aspartic proteases (β-secretase) indicate a rearrangement of the active residues during this step, and a disruption of a hydrogen bond between Ser41 and Tyr83, subsequently to the cleavage of the scissile bond. However, neither the cleavage of the substrate nor this reorganization were observed here, and the network of hydrogen bonds, which was referenced beforehand, between Asp38−Ser41−Tyr83−Trp45, was preserved during this second step.[24,45] A third reaction step was needed to generate the products.

The Third Reaction Step. To generate the products, we carried out a linear transit scan along the distance between each gem-diol proton and the carboxyl oxygen to which it was hydrogen-bonded. The structures of the transition state (TS3) and reaction products (P) were easily obtained and are shown in Figure 3. It was difficult to optimize TS3, and we could not achieve standard convergence criteria. Nevertheless, its nature was verified by the existence of a single imaginary frequency (596*i* cm^{-1}). During the progressive transfer of the gem-diol proton to Asp38, the scissile bond of angiotensinogen elongated and spontaneously broke. In the products, the catalytic aspartates were both protonated and two independent peptides were formed, as expected. This reaction step, which led to the angiotensinogen cleavage, had an activation free energy of 16.5 kcal mol^{-1} (see Figure 4).

Hydrolysis of the Mutated Substrate. Previous studies have linked a specific mutation in angiotensionogen with preeclampsia, which is a common hypertensive disorder of pregnancy. This mutation, at the site of renin cleavage, corresponds to a replacement of a leucine at the 10th position of angiotensinogen for a phenylalanine.[29] Because of this association, computational methods were used also to describe the hydrolysis of this mutated substrate by renin.

The First Reaction Step: Formation of the Gem-Diol Intermediate. The optimized reactants for the mutated substrate were very similar to the wild-type substrate described beforehand. The comparison between the complex renin:wild-type substrate and renin:mutated substrate revealed few differences between the two structures. In fact, the only one resided in the substrate in which a Leu residue was replaced by a Phe residue, at position 10. In the optimized reactants, the catalytic water molecule interacted with the Asp dyad through hydrogen bonds. The same strategy that was used for the previously described mechanism was adopted, and the same reaction coordinates were followed through linear transit scans. In the first reaction step, the distance between the oxygen of the catalytic water molecule and the carbonyl carbon of Phe10 was used as the reaction coordinate. The catalytic water molecule performed a nucleophilic attack on the carbonyl group of the scissile bond concerted with protonation of the carbonyl oxygen by Asp38. The structure of the TS1 was identified and has shown that the distance between the water oxygen and the carbonyl carbon decreased from 3.24 Å to 1.70 Å. There were no significant changes in the residues around the active site, as had already happened in the first described mechanism. In the first transition state, the oxygen of the water molecule and the carbonyl group were slightly closer than in the previous mechanism. The Ser41−Tyr83 hydrogen bond was shorter as well. The larger size of phenylalanine, compared to leucine, may explain these differences. Despite these aspects, the first reaction step was very similar overall to what was described for the reaction with the wild-type substrate. As in the previous mechanism, the protonation of the carbonyl group was completely accomplished at the end of this first step. In the end a gem-diol intermediate was obtained, with the hybridization of the carbonyl carbon changing from sp_2 to sp_3 and, consequently, its geometry from planar to tetrahedral. The network of hydrogen bonds involving the Asp38−Ser41−Tyr83−Trp45 residues remained unchanged. No other significant atomistic differences were found when this mechanism was compared to the reaction with the wild type substrate. In this model, this first step was associated with an activation energy of 15.8 kcal mol^{-1}.

The Second Reaction Step. To study the second step of this reaction, the distance between the peptidic nitrogen and the Asp226 acidic proton was used as reaction coordinate, similar to the previously described mechanism. At the transition state (TS2), the proton was between these two residues (at distances of 1.30 Å to Leu10 nitrogen and 1.23 Å to the oxygen), being completely transferred only at the products of this step (INT2). The peptidic bond was not completely cleaved at INT2 (bond length of 1.57 Å), the catalytic Asp38 remained deprotonated and the amide nitrogen became positively charged. Therefore, a third reaction step was necessary for the complete hydrolysis of the mutated substrate, as opposed to the other aspartic proteases and in agreement with the catalytic mechanism for the wild-type substrate. This reaction needed an activation energy of 12.0 kcal mol^{-1}.

The Third Reaction Step. The reaction coordinate was taken as the distance from a gem-diol proton to the carboxyl oxygen of Asp38, from where we have obtained the structure of the third transition state and the final products. At the end of the reaction cycle, the substrate was hydrolyzed to two independent peptides, in a manner analogous to that of the

dx.doi.org/10.1021/cs500497f | *ACS Catal.* 2014, 4, 3869−3876

wild-type substrate. Therefore, the catalytic reaction mechanism of this mutated substrate was similar to the hydrolysis of the natural substrate. Thus, it was concluded that the Leu10Phe mutation did not cause relevant mechanistic changes in the catalytic cycle or structural changes in the enzyme−substrate interaction. The activation energy for the last step was 16.4 kcal mol^{-1}, which was comparable to the experimental value for this hydrolysis (18.3 kcal mol^{-1}),[44] and this final step led to a very stable dipeptide (reaction energy of −16.2 kcal mol^{-1}).

The energy pathway and the representation of the stationary points for this mechanism are given in the Supporting Information. The overall conclusion is that the catalytic mechanism of the cleavage of angiotensinogen is the same for the wild type and for the preeclampsia-generating mutant. However, we found differences between the barriers of both mechanisms, based on their PES profiles. Experimental barriers are very similar, and the experimental difference is only 1.8 kcal mol^{-1}. This means that the theoretical method used here identifies the correct chemical pathway, albeit facing challenges in retrieving high-accuracy energies.

Human Renin and Mouse Renin. In preclinical trials, the mouse is the standard animal model to test new drug candidates. However, many times, results on mice are not transferable to humans, because of the different physiologies of the two organisms. Therefore, it becomes very important to compare the catalytic mechanisms of both human and mouse renin, in order to predict how reliable the mouse models will be. The hydrolysis catalyzed by mouse submandibular renin was previously described in our group.[46]

Human renin is 68% homologous in amino acid sequence to mouse renin, and the active site of these two enzymes have similar folds. Some differences are observed in only a few residues. In human renin, Ala229 substitutes a threonine residue that is conserved in the most part of the aspartic proteases. This alanine residue lacks the ability to form a hydrogen bond with an aspartate in the active site. In mouse renin, the same threonine is substituted by Ser226. Another difference is observed in Val36, which is in close proximity to one of the catalytic aspartates in human renin. In the mouse enzyme this residue corresponds to an isoleucine, which is not identical but is very similar to the human counterpart.[47]

Comparing our present results with our previous studies in mice, we conclude that both human and mouse renin adopt the same hydrolysis mechanisms, and the same sequence of steps, with similar transition states, to hydrolyze angiotensinogen. We can conclude also that the different residues between these enzymes are not essential to catalysis. In conclusion, the mouse model seems to be reliable to test drug candidates, at least at the level of renin inhibition.

CONCLUSIONS

In this work, we have explored, computationally, the mechanism of angiotensinogen hydrolysis by human renin at the atomic level. The results showed that the transformation was accomplished with the help of acid/base catalysts in three elementary steps, contrary to other proteases of the same family, which perform an identical reaction in just two steps.

The first step is characterized by the formation of a gem-diol intermediate upon nucleophilic attack of a water molecule on the substrate carbonyl. The protonation of the peptidic nitrogen of the hydrolyzed bond takes place in the second reaction step. A third and last step is necessary to the formation of the final product, characterized by the transfer of a gem-diol proton back to the Asp 38, simultaneously with the cleavage of the scissile bond between Leu10 and Val11 of angiotensinogen.

The comparison of the results obtained here for the human enzyme with previous works on the mouse enzyme, led us to conclude that these two mechanisms are very similar. Since mice are usually used as models to preliminarily test drug candidates, this comparison gives further confidence about the transferability of the results obtained in this animal model to humans.

The energy pathway obtained for this mechanism showed that the first reaction step is rate-limiting, with an activation free energy of 22.0 kcal mol^{-1} (M06/6-311++G(2d,2p):AMBER). Similar results were obtained with a set of different density functionals (see Table S1 in the Supporting Information). The experimental value for the hydrolysis of the N-terminal tetradecapeptide of angiotensinogen by renin is 16.5 kcal mol^{-1}.[44] This is comparable to the value obtained in this work, if we take into account the error associated with the methodology.

The results described in this work also showed that the replacement of a leucine by a phenylalanine, in position 10 of the angiotensinogen, did not change the reaction catalyzed by human renin. Therefore, we can conclude that the association of this mutation with preeclampsia should not be related to changes in the hydrolysis mechanism catalyzed by renin. In fact, the difference between the two enzymes is very small but, together with a change in K_M, the enzyme becomes more efficient, which should play a role in hypertension.

Since renin is an essential enzyme for blood pressure control, studies such as the present one are necessary for a better understanding of its role. The complete description of this catalytic mechanism and the atomistic details of its transition state are valuable tools for the rational design of new antihypertensive drugs. The geometry of the transition state for the rate-limiting step can be used as a model for the exploration of new transition-state analogues inhibitors for this enzyme.

ASSOCIATED CONTENT

Supporting Information

The Supporting Information includes the following materials: a zip file containing xyz files of the stationary points; structures of the reactants, intermediates, transition states, and products for the cleavage of the Phe10-Val11 peptide bond of mutated angiotensinogen by human renin (Figure S1); energetic pathway for the hydrolysis reaction of mutated angiotensinogen catalyzed by human renin (Figure S2); and activation and reaction energies for angiotensinogen hydrolysis by human renin calculated with four density functionals and the 6-311++G(2d,2p) basis set (Table S1). This material is available free of charge via the Internet at http://pubs.acs.org.

AUTHOR INFORMATION

Corresponding Author

*E-mail: mjramos@fc.up.pt.

Notes

The authors declare no competing financial interest.

ACKNOWLEDGMENTS

This work received financial support from the European Union (FEDER funds through COMPETE) and National Funds (FCT, Fundação para a Ciência e Tecnologia) through Project

Nos. PTDC/QUI-QUI/121744/2010, EXCL/QEQ-COM/0394/2012 and Pest-C/EQB/LA0006/2013.

■ ABBREVIATIONS

ACE, angiotensin converting enzyme; AngI, angiotensin I; AngII, angiotensin II; AT1, angiotensin receptors Type 1; AT2, angiotensin receptors Type 2; DFT, density functional theory; INT, intermediate; MD, molecular dynamics; P, product; PES, potential energy surface; QM/MM, quantum mechanics/molecular mechanics; R, reactants; RAS, renin angiotensin system; TS, transition state

■ REFERENCES

(1) Bezencon, O.; Bur, D.; Weller, T.; Richard-Bildstein, S.; Remen, L.; Sifferlen, T.; Corminboeuf, O.; Grisostomi, C.; Boss, C.; Prade, L.; Delahaye, S.; Treiber, A.; Strickner, P.; Binkert, C.; Hess, P.; Steiner, B.; Fischli, W. *J. Med. Chem.* **2009**, *52*, 3689−3702.
(2) Blundell, T.; Sibanda, B. L.; Pearl, L. *Nature* **1983**, *304*, 273−275.
(3) Eder, J.; Hommel, U.; Cumin, F.; Martoglio, B.; Gerhartz, B. *Curr. Pharm. Des.* **2007**, *13*, 271−285.
(4) MacGregor, G. A.; Markandu, N. D.; Roulston, J. E.; Jones, J. C.; Morton, J. J. *Nature* **1981**, *291*, 329−331.
(5) Rahuel, J.; Rasetti, V.; Maibaum, J.; Rueger, H.; Goschke, R.; Cohen, N. C.; Stutz, S.; Cumin, F.; Fuhrer, W.; Wood, J. M.; Grutter, M. G. *Chem. Biol.* **2000**, *7*, 493−504.
(6) Verdecchia, P.; Angeli, F.; Mazzotta, G.; Gentile, G.; Reboldi, G. *Vasc. Health Risk Manage.* **2008**, *4*, 971−981.
(7) Campbell, D. J. *JRAAS* **2012**, *13*, 314−316.
(8) Campbell, D. J.; Alexiou, T.; Xiao, H. D.; Fuchs, S.; McKinley, M. J.; Corvol, P.; Bernstein, K. E. *Hypertension* **2004**, *43*, 854−859.
(9) Dinh, D. T.; Frauman, A. G.; Johnston, C. I.; Fabiani, M. E. *Clin. Sci. (London)* **2001**, *100*, 481−492.
(10) Crowley, S. D.; Coffman, T. M. *Exp. Cell Res.* **2012**, *318*, 1049−1056.
(11) Katsurada, A.; Hagiwara, Y.; Miyashita, K.; Satou, R.; Miyata, K.; Ohashi, N.; Navar, L. G.; Kobori, H. *Am. J. Physiol. Renal Physiol.* **2007**, *293*, F956−960.
(12) Cumin, F.; Le-Nguyen, D.; Castro, B.; Menard, J.; Corvol, P. *Biochim. Biophys. Acta* **1987**, *913*, 10−19.
(13) Tice, C. M. *Annu. Rep. Med. Chem.* **2006**, *41*, 155.
(14) Jensen, C.; Herold, P.; Brunner, H. R. *Nat. Rev. Drug Discovery* **2008**, *7*, 399−410.
(15) Pilz, B.; Shagdarsuren, E.; Wellner, M.; Fiebeler, A.; Dechend, R.; Gratze, P.; Meiners, S.; Feldman, D. L.; Webb, R. L.; Garrelds, I. M.; Jan Danser, A. H.; Luft, F. C.; Muller, D. N. *Hypertension* **2005**, *46*, 569−576.
(16) Wood, J. M.; Maibaum, J.; Rahuel, J.; Grutter, M. G.; Cohen, N. C.; Rasetti, V.; Ruger, H.; Goschke, R.; Stutz, S.; Fuhrer, W.; Schilling, W.; Rigollier, P.; Yamaguchi, Y.; Cumin, F.; Baum, H. P.; Schnell, C. R.; Herold, P.; Mah, R.; Jensen, C.; O'Brien, E.; Stanton, A.; Bedigian, M. P. *Biochem. Biophys. Res. Commun.* **2003**, *308*, 698−705.
(17) Sielecki, A. R.; Hayakawa, K.; Fujinaga, M.; Murphy, M. E. P.; Fraser, M.; Muir, A. K.; Carilli, C. T.; Lewicki, J. A.; Baxter, J. D.; James, M. N. G. *Science* **1989**, *243*, 1346−1351.
(18) Gradman, A. H.; Kad, R. *J. Am. Coll. Cardiol.* **2008**, *51*, 519−528.
(19) Nakagawa, T.; Akaki, J.; Satou, R.; Takaya, M.; Iwata, H.; Katsurada, A.; Nishiuchi, K.; Ohmura, Y.; Suzuki, F.; Nakamura, Y. *Biol. Chem.* **2007**, *388*, 237−246.
(20) Gorfe, A. A.; Caflisch, A. *Structure* **2005**, *13*, 1487−1498.
(21) Politi, A.; Durdagi, S.; Moutevelis-Minakakis, P.; Kokotos, G.; Papadopoulos, M. G.; Mavromoustakos, T. *Eur. J. Med. Chem.* **2009**, *44*, 3703−3711.
(22) Sibanda, B. L.; Blundell, T.; Hobart, P. M.; Fogliano, M.; Bindra, J. S.; Dominy, B. W.; Chirgwin, J. M. *FEBS Lett.* **1984**, *174*, 102−111.
(23) Bras, N. F.; Fernandes, P. A.; Ramos, M. J. *J. Biomol. Struct. Dyn.* **2014**, *32*, 351−363.
(24) Barman, A.; Prabhakar, R. *J. Mol. Graph. Model.* **2013**, *40*, 1−9.
(25) Piana, S.; Bucher, D.; Carloni, P.; Rothlisberger, U. *J. Phys. Chem. B* **2004**, *108*, 11139−11149.
(26) Cascella, M.; Micheletti, C.; Rothlisberger, U.; Carloni, P. *J. Am. Chem. Soc.* **2005**, *127*, 3734−3742.
(27) Garrec, J.; Sautet, P.; Fleurat-Lessard, P. *J. Phys. Chem. B* **2011**, *115*, 8545−8558.
(28) Hong, L.; Tang, J. *Biochemistry* **2004**, *43*, 4689−4695.
(29) Inoue, I.; Rohrwasser, A.; Helin, C.; Jeunemaitre, X.; Crain, P.; Bohlender, J.; Lifton, R. P.; Corvol, P.; Ward, K.; Lalouel, J. M. *J. Biol. Chem.* **1995**, *270*, 11430−11436.
(30) Zhou, A.; Carrell, R. W.; Murphy, M. P.; Wei, Z.; Yan, Y.; Stanley, P. L.; Stein, P. E.; Broughton Pipkin, F.; Read, R. J. *Nature* **2010**, *468*, 108−111.
(31) Case, D. A.; Darden, T. A.; Cheatham, T. E., III; Simmerling, C. L.; Wang, J.; Duke, R. E.; Luo, R.; Crowley, M.; Walker, R. C.; Zhang, W.; Merz, K. M.; Wang, B.; Hayik, S.; Roitberg, A.; Seabra, G.; Kolossváry, I.; Wong, K. F.; Paesani, F.; Vanicek, J.; Wu, X.; Brozell, S. R.; Steinbrecher, T.; Gohlke, H.; Yang, L.; Tan, C.; Mongan, J.; Hornak, V.; Cui, G.; Mathews, D. H.; Seetin, M. G.; Sagui, C.; Babin, V.; Kollman, P. A. *AMBER 10*; University of California, San Francisco, CA, 2008.
(32) Frisch, M. J.; Trucks, G. W.; Schlegel, H. B.; Scuseria, G. E.; Robb, M. A.; Cheeseman, J. R.; Scalmani, G.; Barone, V.; Mennucci, B.; Petersson, G. A.; Nakatsuji, H.; Caricato, M.; Li, X.; Hratchian, H. P.; Izmaylov, A. F.; Bloino, J.; Zheng, G.; Sonnenberg, J. L.; Hada, M.; Ehara, M.; Toyota, K.; Fukuda, R.; Hasegawa, J.; Ishida, M.; Nakajima, T.; Honda, Y.; Kitao, O.; Nakai, H.; Vreven, T.; Montgomery, J. A., Jr.; Peralta, J. E.; Ogliaro, F.; Bearpark, M.; Heyd, J. J.; Brothers, E.; Kudin, K. N.; Staroverov, V. N.; Kobayashi, R.; Normand, J.; Raghavachari, K.; Rendell, A.; Burant, J. C.; Iyengar, S. S.; Tomasi, J.; Cossi, M.; Rega, N.; Millam, J. M.; Klene, M.; Knox, J. E.; Cross, J. B.; Bakken, V.; Adamo, C.; Jaramillo, J.; Gomperts, R.; Stratmann, R. E.; Yazyev, O.; Austin, A. J.; Cammi, R.; Pomelli, C.; Ochterski, J. W.; Martin, R. L.; Morokuma, K.; Zakrzewski, V. G.; Voth, G. A.; Salvador, P.; Dannenberg, J. J.; Dapprich, S.; Daniels, A. D.; Farkas, Ö.; Foresman, J. B.; Ortiz, J. V.; Cioslowski, J.; Fox, D. J. *Gaussian 09*; Gaussian, Inc.: Wallingford, CT, 2009.
(33) Vreven, T.; Byun, K. S.; Komáromi, I.; Dapprich, S.; Montgomery, J. A.; Morokuma, K.; Frisch, M. J. *J. Chem. Theory Comput.* **2006**, *2*, 815−826.
(34) Becke, A. D. *J. Chem. Phys.* **1993**, *98*, 5648−5652.
(35) Kohn, W.; Becke, A. D.; Parr, R. G. *J. Phys. Chem.* **1996**, *100*, 12974−12980.
(36) Lee, C.; Yang, W.; Parr, R. G. *Phys. Rev. B* **1988**, *37*, 785.
(37) Bayly, C. I.; Cieplak, P.; Cornell, W. D.; Kollman, P. A. *J. Phys. Chem.* **1993**, *97*, 10269−10280.
(38) Besler, B. H.; Merz, K. M.; Kollman, P. A. *J. Comput. Chem.* **1990**, *11*, 431−439.
(39) Singh, U. C.; Kollman, P. A. *J. Comput. Chem.* **1984**, *5*, 129−145.
(40) Brás, N. F.; Fernandes, P. A.; Ramos, M. J. *J. Chem. Theory Comput.* **2010**, *6*, 421−433.
(41) Oliveira, E. F.; Cerqueira, N. M. F. S. A.; Fernandes, P. A.; Ramos, M. J. *J. Am. Chem. Soc.* **2011**, *133*, 15496−15505.
(42) Ribeiro, A. J. M.; Ramos, M. J.; Fernandes, P. A. *J. Am. Chem. Soc.* **2012**, *134*, 13436−13447.
(43) Carnevale, V.; Raugei, S.; Piana, S.; Carloni, P. *Comput. Phys. Commun.* **2008**, *179*, 120−1230.
(44) Pilote, L.; McKercher, G.; Thibeault, D.; Lamarre, D. *Biochem. Cell Biol.* **1995**, *73*, 163−170.
(45) Barman, A.; Schurer, S.; Prabhakar, R. *Biochemistry* **2011**, *50*, 4337−4349.
(46) Bras, N. F.; Ramos, M. J.; Fernandes, P. A. *Phys. Chem. Chem. Phys.* **2012**, *14*, 12605−12613.
(47) Hobart, P. M.; Fogliano, M.; O'Connor, B. A.; Schaefer, I. M.; Chirgwin, J. M. *Proc. Natl. Acad. Sci. U. S. A.* **1984**, *81*, 5026−5030.